Eur. Phys. J. B **27**, 119–126 (2002)
DOI: 10.1140/epjb/e20020136

THE EUROPEAN PHYSICAL JOURNAL B
EDP Sciences

Electronic structure and anomalous physical properties of metastable Al-Si solid solutions

D.V. Livanov[1,a], E.I. Isaev[1], Yu.Kh. Vekilov[1], S.I. Manokhin[1], A.S. Mikhaylushkin[1], and S.I. Simak[2]

[1] Department of Theoretical Physics, Moscow State Institute of Steel and Alloys - Technological University, Leninsky pr. 4, 119991 Moscow, Russia
[2] Department of Applied Physics, Chalmers University of Technology and Göteborg University, SE-412 96 Gothenburg, Sweden

Received 31 January 2002

Abstract. Al-Si solid solutions synthesized under high pressure demonstrate striking physical properties, such as enhanced superconductivity and peculiarities of low-temperature transport coefficients. In order to understand the connection of these effects to the electronic structure changes we have performed a first-principles study of the electronic spectra and Fermi surfaces of Al-Si solid solutions. We show that two electronic topological transitions (ETT's) lead to unusual concentration dependencies of the resistivity, thermoelectric power and Hall constant of the system while a variety of other interesting phenomena such as lattice instability and superconductivity enhancement may be a result of the nesting features appearing upon Si doping. We present also the results of our theoretical calculations of the thermodynamic and transport properties of Al-Si solid solutions which are in good agreement with experiment and reproduce nicely the experimentally observed peculiarities.

PACS. 72.10.-d Theory of electronic transport; scattering mechanisms

1 Introduction

Al-rich $Al_{1-x}Si_x$ substitutional solid solutions with the face-centered cubic (fcc) structure demonstrate unusual physical properties. In particular, rather peculiar behavior of the low-temperature thermoelectric power and Hall constant and an increase of the superconducting critical temperature, T_c, by an order of magnitude compared to pure Al have been observed in recent experiments [1–9]. Silicon is poorly dissolved in aluminum at ambient conditions and in order to reach the Si content $x \sim 0.1$, the synthesis under high pressure (up to 8 GPa) followed by the quenching to liquid nitrogen temperatures is required. So obtained non-equilibrium solid solutions $Al_{1-x}Si_x$ are homogeneous single-phase compounds with T_c increasing from 1.18 K for $x = 0$ (pure Al) up to 11 K for $x \approx 0.2$. Rather simple Fermi surface composed of the s- and p-electronic states and an almost linear dependence of T_c on the Si content make these materials an excellent model superconductor for investigations of the interplay between superconductivity and the lattice instability.

The nonequilibrium state with remarkable lattice instability is a direct consequence of the supersaturation of $Al_{1-x}Si_x$ solid solutions. As it was first demonstrated in references [2,3], an essential softening of the transverse acoustic phonon modes and decrease of the shear modulus with Si doping are the main reasons behind dramatic enhancement of superconductivity in $Al_{1-x}Si_x$. Later on anomalies in transport properties such as thermoelectric power and Hall constant were found [5,7,8] in the vicinity of the lattice instability point. It was also argued that the enhancement of superconductivity is connected to the increase of the electron-phonon matrix element [6].

Here we present the results of our first-principles calculations of the Fermi surfaces and electronic properties of $Al_{1-x}Si_x$ solid solutions for a wide range of concentrations and pressures revealing physics behind anomalous properties of these compounds. We demonstrate that the electronic structure of pure Al is essentially modified upon Si doping. There are two main features in the electronic structure which result in a variety of anomalies. First, there are two electronic topological transitions (ETT's) taking place with increasing concentration of Si and/or pressure. Further we demonstrate that one of these ETT's has to be responsible for the experimentally observed anomalies in transport properties. Second, we find the effect of gradual flattening of the Fermi surface parts with increasing concentration of Si. We identify pronounced nesting features of the Fermi surface related to this flattening and trace down their dependence on the Si concentration.

The paper is structured as follows. In Section 2 we present the details of our computational technique. Section 3 is devoted to the calculation of the electronic structure of $Al_{1-x}Si_x$ solid solutions. We present the details of the Fermi surface at different Si concentrations and

[a] e-mail: d.livanov@misis.ru

pressures and find two ETT's taking place in the system. Then we provide an evidence for nesting features and trace down their dependence on Si concentration. Section 4 is devoted to the calculation of the thermodynamic properties of $Al_{1-x}Si_x$ substitutional solid solutions: formation enthalpy, lattice parameter, bulk modulus as well as one-electron density of states at the Fermi level. In Section 5 we discuss the transport properties of the system such as resistivity, thermoelectric power and Hall constant and demonstrate the connection between anomalies of transport properties and an ETT which takes place upon Si doping. The results are summarized in Section 6.

2 Computational details

The scalar-relativistic KKR-CPA-ASA [10] method with a basis set consisting of s, p and d orbitals was used to study random Al-Si solid solutions on the fcc underlying lattice. Exchange and correlation were included within the density functional theory making use of the Perdew-Burke-Erzernhof generalized gradient approximation (GGA) [11]. The atomic sphere radii for both elements were chosen equal to the radius of the average atomic Wigner-Sietz sphere of the solid solution, and the charge transfer effects were included in the framework of the screened impurity model with a prefactor $\beta = 0.6$ [12]. The Brillouin zone integration was performed by employing the special points technique and using up to 1500 k-points in the irreducible wedge of the fcc Brillouin zone (BZ). The energy integrals were calculated on a semicircular complex energy contour with 25 points on it. The convergence criterion for the total energy was 0.001 mRy. To obtain the ground state properties of the solid solutions we performed GGA self-consistent calculations for a large number of concentrations of Si between 0 and 100 at.% with different lattice parameters, and subsequently used a Morse-like fitting for the total energy curves [13]. The Fermi surfaces (FS) were calculated on the basis of the formalism presented in detail in reference [14] by mapping the maxima of the Bloch spectral density function $A(k, E_F)$ onto the BZ. The FS presented in the following section were calculated on the dense grid of k-points in the ΓXWK section of the fcc BZ for the lattice parameters corresponding to different concentrations and pressures.

3 Fermi surface

3.1 Electronic topological transitions

The FS of pure aluminum at ambient conditions consists of a big second-zone hole part and a small third-zone toroidlike electron pocket around point K, as shown in Figure 1. When applying moderate pressure to pure aluminum the effect is mainly the shrinkage of the electron pocket at K. At pressure higher than 8 GPa this pocket finally disappears, what corresponds to the ETT of the void disappearance type. As should be expected, alloying

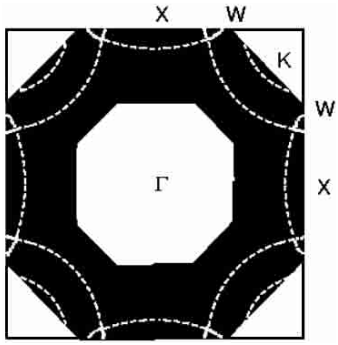

Fig. 1. Calculated Fermi surface of pure aluminum at zero pressure.

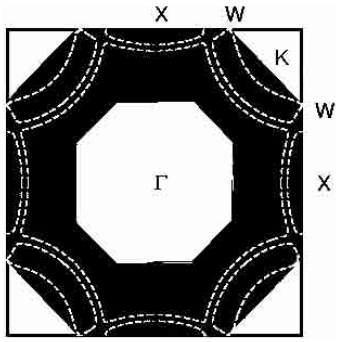

Fig. 2. Calculated Fermi surface of random alloy Al + 10 at.% of Si at zero pressure.

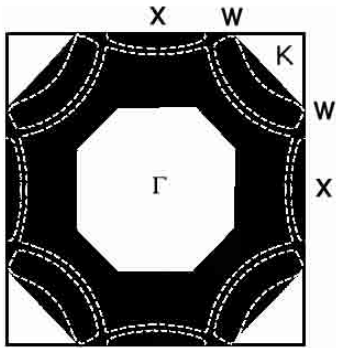

Fig. 3. Calculated Fermi surface of random alloy Al + 8 at.% of Si at $P = 8$ GPa.

with Si, whose number of valence electrons is higher by one compared to Al, has an opposite effect on the development of the electron pocket at K. The pocket grows with increasing Si content resulting in the ETT of the neck formation type taking place near point W at 10 at.% of Si at zero pressure (see Fig. 2). Higher pressure, however, facilitates the neck formation and at about 8 GPa this ETT takes place already at 8 at.% of Si (see Fig. 3). It should be mentioned that the analysis of the FS development has been done for the whole BZ and the above mentioned ETT's are the only ones found for the ranges of concentrations and pressures addressed in this work. According to the general theory of ETT's [18] they have to manifest themselves in the peculiarities of different physical properties, first of all transport properties, such as the

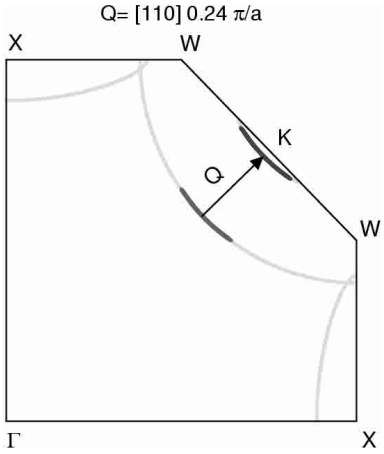

Fig. 4. Calculated part of the Fermi-surface of pure Al. Parts of the Fermi surface connected by the nesting vector **Q** are emphasized (a detailed explanation is given in the text).

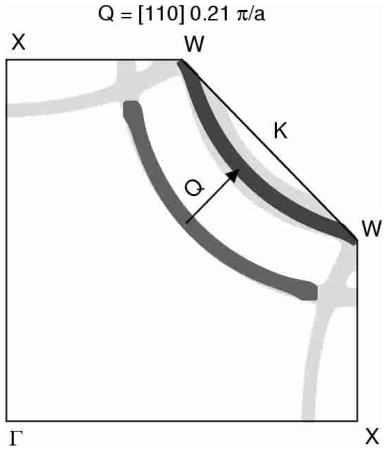

Fig. 5. Calculated part of the Fermi-surface of alloy Al + 20 % at. Si. Parts of the Fermi surface connected by the nesting vector **Q** are emphasized (a detailed explanation is given in the text).

thermoelectric power. Certainly, the second ETT of the neck formation type is of most interest as it takes place with increasing Si content and therefore may be considered in the context of recent experiments on the concentration dependences of transport properties of Al-Si solid solutions. The fact that the experimentally measured thermoelectric power demonstrates a pronounced peculiarity at about 8–10 at.% of Si [7] agrees nicely with the presence of an ETT in the same range of the Si content. On the other hand, it follows from the microscopic theory of ETT's [18], that they do not influence the superconducting properties, at least for three-dimensional systems.

3.2 Nesting features and enhanced superconductivity

Fermi surface nesting features (Kohn anolmalies) are known to lead to a variety of instabilities including Peierls, charge-density-wave and spin-density-wave instabilities. Kohn [15] has shown that for a free electron gas, the existence of a sharp Fermi surface leads to non-analyticities in the wave-vector dependent quantities such as phonon spectrum, susceptibility etc. Later on, these results were generalized for the case of an arbitrary band structure, particularly, nesting features. It has also been argued that high superconducting transition temperatures of various compounds may arise from different kinds of instabilities [16,17].

To analyze the possible nesting features and trace down their dependence on the Si content we calculated products of the Bloch spectral functions $(A(\mathbf{k}, E_F)A(\mathbf{k}+\mathbf{Q}, E_F))$ at points $\mathbf{k}$ and $\mathbf{k}+\mathbf{Q}$, where $\mathbf{k}$ belongs to the first BZ and $\mathbf{Q}$ is the so-called Fermi surface superposition vector. Quantity of $A(\mathbf{k}, E_F)A(\mathbf{k}+\mathbf{Q}, E_F)$ has the meaning of the weight of the local superposition of two Fermi surface parts when BZ is displaced by vector $\mathbf{Q}$. Quite obviously it attains a non-zero value only when the nesting corresponding to vector $\mathbf{Q}$ is present and therefore helps to reveal the nesting features of a system.

Fermi surface calculations show that the essential imposition of the two symmetrical parts of the second hole zone and third electron zone takes place in the system. In Figures 4 and 5 the nesting vector $\mathbf{Q}$ connecting the second hole zone and the third electron zone in pure Al and $Al_{0.8}Si_{0.2}$ alloys is clearly seen. It should be noticed that upon increase of the Si content the nesting feature of the FS becomes gradually more pronounced due to both growth of the third electron zone and the FS smearing typical of disordered alloys. Though the quantitative analysis of the interplay between nesting features and superconductivity is beyond the scope of the present article, we mention that nesting may be responsible for appearance of the soft mode in the phonon spectrum and hence the enhancement of superconductivity in $Al_{1-x}Si_x$ substitutional alloys.

The dramatic increase of the superconducting critical temperature, T_c upon Si doping is one of the most remarkable features of $Al_{1-x}Si_x$ substitutional solid solutions. The superconducting critical temperature was found to increase by an order of magnitude (from 1.18 K to 11 K) with variation of Si content in a series of homogeneous single-phase fcc metallic compounds. Moreover, $Al_{1-x}Si_x$ solid solutions can be considered as a very interesting object for studies of the interplay between the superconducting properties and the lattice instability in metallic systems. A simple Fermi surface composed of the *s*- and *p*-electronic states allows for a simple relation between T_c and Si content [9] to be used and provides the possibility to consider these alloys as a very promising model system to study the mechanism of superconductivity enhancement in the vicinity of the lattice instability.

Due to the above mentioned reasons we discuss qualitatively the possible relationship between nesting features and superconductivity in this compound. It was found in recent studies [6], that if both the one-electron density of states at Fermi level and the phonon spectrum parameters are only slightly dependent upon composition, their change with Si doping can provide just 1–3 % change

in T_c. Therefore, the only direct reason for an order of magnitude increase of the superconducting critical temperature may be the enhancement of the electron-phonon coupling λ with the Si doping. Discussing the possible influence of Si doping on λ, one has to distinguish the effects of modifications of the electron and phonon spectra parameters. Although some phonon softening was discovered in reference [3], it was shown not to be sufficient to provide an order of magnitude increase of T_c [6]. Therefore, it is the change in the electronic structure which should be responsible for the anomalous increase of of the electron-phonon interaction and T_c. As was demonstrated above the analysis of the Fermi surface transformation under Si doping allows us to identify the nesting features of the Fermi surface. Qualitatively these nesting features may result in an anomalous increase of the one-electron susceptibility with Si content at nesting vectors $\mathbf{Q}$ with the corresponding enhancement of the electron-phonon interaction. The results of first-principle calculations of the one-electron susceptibility as well as numerical estimation of the electron-phonon coupling constant will be reported elsewhere.

4 Thermodynamic properties

4.1 Formation enthalpy

The formation enthalpy of Al-Si random alloys ($\Delta H(\mathrm{Al}_{1-x}\mathrm{Si}_x)$) was calculated as a measure of the stability of the system with respect to the phase separation into pure aluminum and silicon in their ground state fcc and diamond structures, respectively. Therefore $\Delta H(\mathrm{Al}_{1-x}\mathrm{Si}_x) = H(\mathrm{Al}_{1-x}\mathrm{Si}_x) - xH(\mathrm{Si}) - (1-x)H(\mathrm{Al})$, where $H = E + PV$, with E standing for the total energy, P for the pressure, and V for the volume. The results are presented in Figure 6. ΔH is exactly zero at $x = 0$ as it corresponds to the pure Al in the fcc structure and has a positive value at $x = 1$ corresponding to the enthalpy difference between silicon in the diamond and fcc structures. From the character of the curve it is obvious that Al-Si random alloys at ambient conditions are unstable with respect to the phase separation in the whole concentration interval. This agrees well with an experimental phase diagram suggesting extremely limited low temperature solubility of Si in Al matrix (0.3% according to reference [19]). Under pressure, however, the relative stability of the random Al-Si alloys with respect to the elemental Al and Si gradually increases and already at $P \sim 6.5$ GPa the solubility of Si in Al reaches ~ 25 at.%. It reproduces nicely the result of experimental observations [7]. At pressures higher than 9 GPa the solubility becomes unlimited. We note, however, that there is a phase transition in Si from the diamond to the β-Sn structure, which is experimentally found in the range 8.8–12.5 GPa [20,21]. We did not consider the β-Sn structure in our analysis and did not compare the enthalpies of the diamond and β-Sn structures due to the limited accuracy of our calculational technique based on the ASA approximation. We remark, however, that due to such a phase transition, one should expect that at highest pressures considered in the present work some decrease of the solubility limits should occur.

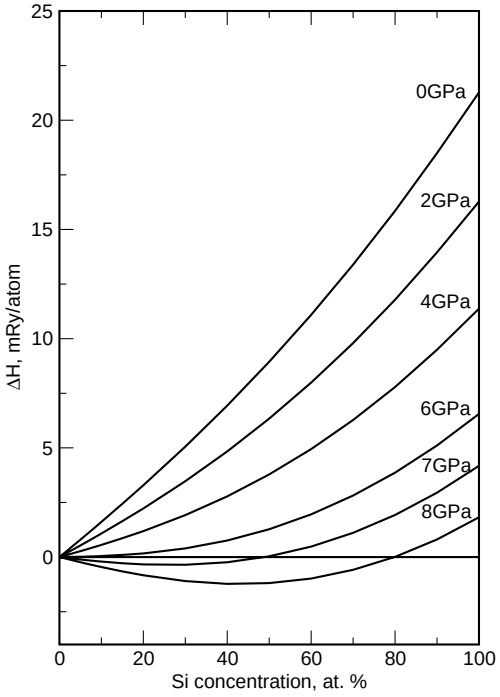

Fig. 6. Calculated formation enthalpy as a function of Si content.

4.2 Lattice parameter and bulk modulus

The calculated lattice parameter as a function of Si content is presented in Figure 7 together with the experimental data from references [22,23]. The calculated values are found in good agreement with experimental ones. The lattice parameter is decreasing with increasing Si concentration with a deviation from the Vegard's law to be practically negligible. We note, that the fact that a good description of the behavior of the lattice parameter with increasing Si concentration indicates indirectly that the crystal structure and atomic distribution of the experimentally investigated Al-Si alloys should be rather close to those of an idealized fcc random alloys considered here. Otherwise any pronounced clustering of Si would result in the essential deviation of the lattice parameter from the Vegard's law due to a strong volume relaxation (atomic volumes of Si in the diamond and fcc structures are differ by $\sim 16\%$).

The concentration dependence of the calculated bulk modulus is presented in Figure 8. The calculated bulk modulus of the pure fcc Al is 94.6, in reasonable agreement with experimental value of 76 GPa [24]. It moderately decreases with increasing Si content (by just 1.5% at 15 at.% of Si compared to pure Al) and reveals a kink in the range 6–10 at.% , with a minimum near 6 at.% of Si content and a maximum near 10 at.% of Si. Theoretically the influence of ETT on the bulk modulus has not been

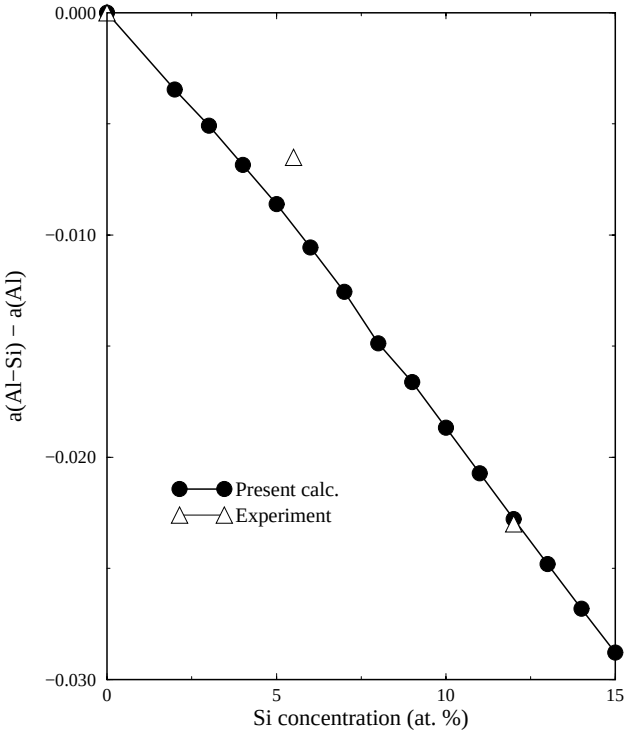

Fig. 7. Calculated lattice parameter as a function of Si content and experimental data from references [22, 23].

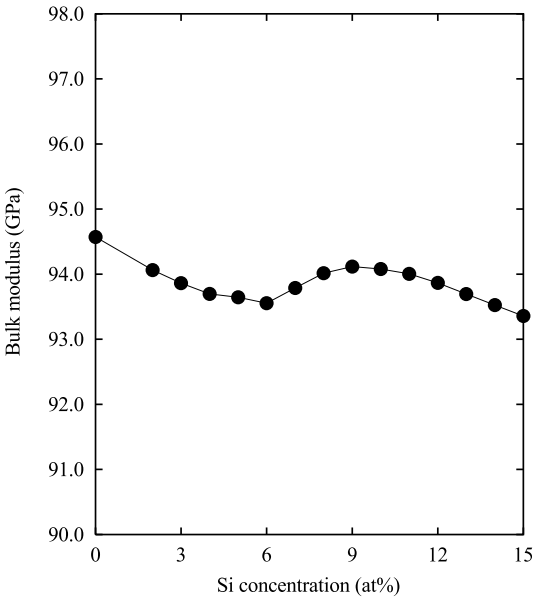

Fig. 8. Calculated bulk modulus as a function of Si content.

studied in detail. From general expectations one may argue that an anomaly in the bulk modulus connected with the ETT must be of the same cusp-like type as in other thermodynamical properties (heat capacity, compressibility and so on) and electrical resistivity [25].

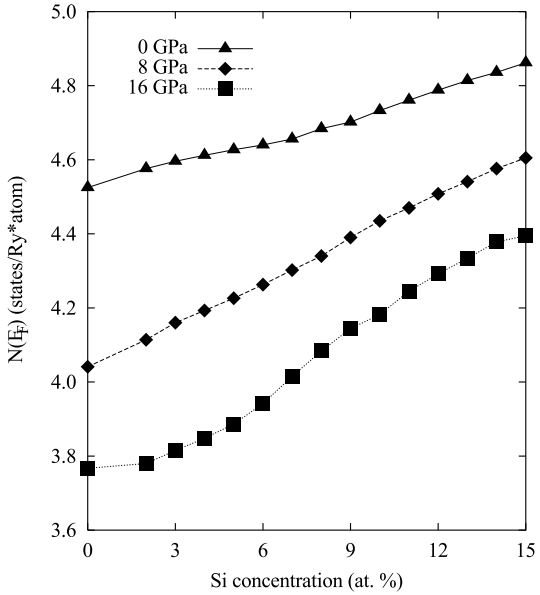

Fig. 9. Calculated density of states at Fermi level as a function of Si content.

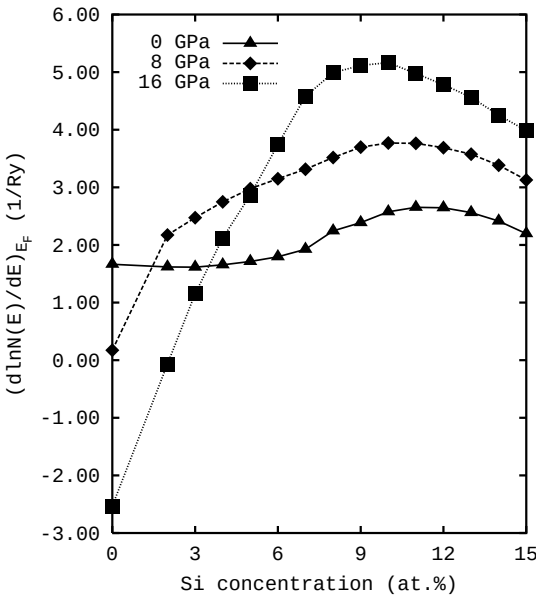

Fig. 10. Calculated derivative of the density of states at Fermi level with respect to energy as a function of Si content.

4.3 Density of states

The density of states was calculated for 15 Al-Si solid solutions with Si content ranging from 0 to 15 at.% and volumes corresponding to pressures ranging from 0 to 16 GPa. A very fine grid of k-points was used for the integration over the Brillouin zone. Derivatives of the density of state at the Fermi level were obtained by an accurate numerical differentiation. Results of first-principles calculations of $N(E_F)$ and $[\mathrm{d}N(E)/\mathrm{d}E]_{E=E_F}$ at various Si concentrations are presented in Figures 9 and 10, respectively.

5 Transport properties

In a large number of metals and metallic alloys, the topological properties of the Fermi surface may change under the influence of different factors such as chemical composition, pressure and so on (for a comprehensive review, see Ref. [18]). The cusps in the heat capacity, magnetic susceptibility and electrical conductivity as well as singularities in the thermoelectric power were observed in different metallic systems as functions of the energy Δ characterizing the proximity of the system to the topological transition point. To describe the transition of the neck disruption or the neck formation type, the simplest model of the Fermi surface in the form of rotation hyperboloid has been introduced [18]. If the chemical potential of the electrons changes under the influence of pressure, deformation or chemical composition, this model describes the transformation of a one-sheet hyperboloid ($\Delta > 0$) into a two-sheet hyperboloid ($\Delta < 0$) (from the former to the latter for the neck disruption and *vice versa* for the neck formation type ETT's, respectively).

The conductivity, σ, the thermoelectric power, S, and Hall constant, R in a metallic system are given by [26,27]:

$$\sigma = \frac{1}{3} e^2 [v_F^2 \tau N]_{E=E_F}, \tag{1}$$

$$S = \frac{1}{3e} \frac{1}{[v_F^2 \tau N]_{E=E_F}} \left[\frac{\partial (v_F^2 \tau N)}{\partial E} \right]_{E=E_F}, \tag{2}$$

$$R = \frac{6}{5e} \frac{1}{[v_F^4 N^2]_{E=E_F}} \left[\frac{\partial (v_F^4 N)}{\partial E} \right]_{E=E_F}, \tag{3}$$

where e stands for electron charge, v_F for the Fermi velocity, τ for the relaxation time, and E_F for the Fermi energy. In real solid solutions, σ, S and R are sensitive to the peculiarities of the electron spectrum as well as the relaxation time, and one has to be careful when comparing results from the above equations with experimental data. To evaluate the electrical conductivity one has to know $N(E)$ and $\tau(E)$ at the Fermi level. The situation is more complicated in the case of the thermoelectric power and Hall effects as these transport properties involve the so-called electron-hole asymmetry factors which contain energy derivatives of the density of states, $[\mathrm{d}N(E)/\mathrm{d}E]_{E=E_F}$, and relaxation time, $[\mathrm{d}\tau/\mathrm{d}E]_{E=E_F}$.

It is obvious that for an adequate evaluation of relevant transport properties, one has to know the behavior of the density of states and its derivative as well as the relaxation time and its derivative as a function of Si content. The first-principles methods allow one to evaluate the electron spectrum, shape of the Fermi surface, electronic density of states and other thermodynamic properties. On the other hand, when calculating transport coefficients, one has to know the relaxation time of charge and heat carriers, even if the simplest transport theory is used. To verify quantitatively the relation between the ETT and transport properties we performed theoretical calculations of relevant transport properties of $Al_{1-x}Si_x$ solid solutions in the vicinity of the ETT. As we will show below, despite the fact that both, $N(E_F)$ and $[\mathrm{d}N(E)/\mathrm{d}E]_{E=E_F}$, as functions of Si content resemble the behavior of the resistivity and thermoelectric power respectively, fittings to calculated concentration dependencies of the density of states and its derivative demonstrate that peculiarities in experimentally measured transport properties cannot be completely accounted for, and therefore calculations of the electron relaxation time and its derivative are required. As it was demonstrated in the theory of ETT's [18], it is the peculiarity in the electronic relaxation time, $\tau(E, \Delta)$, in the vicinity of the ETT point which is mainly responsible for anomalies of transport coefficients in alloys, while features of the density of states and its derivative at the Fermi level are of minor importance. Therefore, to describe consistently available experimental data one has to combine the results of first-principles calculations of the Fermi surfaces (to define the precise position of the ETT point) and $[N(E)]_{E=E_F}$ and $[\mathrm{d}N(E)/\mathrm{d}E]_{E=E_F}$ with model calculations of $\tau(E, \Delta)$ and $[\mathrm{d}\tau(E, \Delta)/\mathrm{d}E]_{E=E_F}$ near the ETT point.

For an ETT of the neck disruption type, the electron relaxation time is given by [18]:

$$\tau^{-1}(E, \Delta) = \tau_0^{-1} \frac{\kappa(E - E_F) - \kappa(E + \Delta)}{2E_F}, \tag{4}$$

where

$$\kappa(E) = \sqrt{2} \sqrt{\sqrt{E^2 + \frac{1}{4\tau_0^2}} - E} \tag{5}$$

and τ_0 is the electron relaxation time far from the transition point.

When comparing the results from equations (1–3) as functions of Si content with available experimental data we have used the data for $[N(E)]_{E=E_F}$ and $[\mathrm{d}N/\mathrm{d}E]_{E=E_F}$ calculated by the KKR-CPA method as described above. $[\tau(E)]_{E=E_F}$ and $[\mathrm{d}\tau/\mathrm{d}E]_{E=E_F}$ were calculated from equation (4) and its derivative with respect to energy. Dependence on the Si content, C_{Si}, was incorporated through the parameter Δ: $\Delta = A\, E_F (C_{\mathrm{Si}} - C_{\mathrm{Si}}^{(0)})$, where A is a dimensionless constant and $C_{\mathrm{Si}}^{(0)}$ is the Si content corresponding to the ETT point. According to our first-principles calculations $C_{\mathrm{Si}}^{(0)}$=0.1 was chosen. To account correctly for the Si content dependence we also included it in τ_0. As the electron relaxation time far from the transition point is proportional to the scattering centers concentration, $\tau_0 \propto (C_{\mathrm{Si}} + D)$, where D represents the content of other defects scattering electrons: dislocations, vacancies and so on. Further, in a generally accepted way we assumed that v_F^2 is proportional to C_{Si}, describing the shift of the Fermi energy by Si doping.

Under the above conditions, the electrical conductivity, thermoelectric power and Hall constant were evaluated from equations (1–3) and fitted to the experimental data from reference [7]. Fitting results are shown in Figures 11, 12 and 13. Discussing the results presented in these Figures we have to mention the crucial importance of taking into account peculiarities of the electronic relaxation time in equation (1). Indeed, the dependence of the

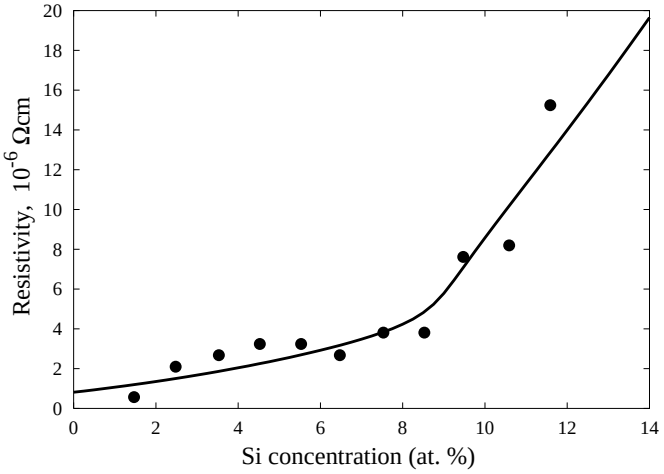

Fig. 11. Calculated resistivity as a function of Si content: the circles are experimental data from reference [7], solid line is a fit.

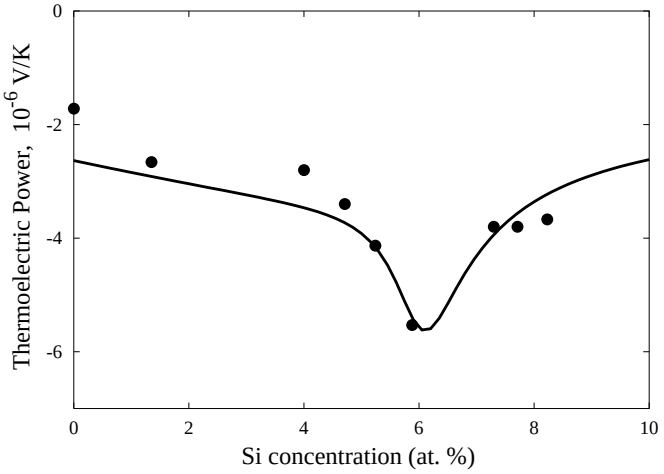

Fig. 12. Calculated thermopower as a function of Si content: the circles are experimental data from reference [7], solid line is a fit.

density of states at the Fermi level upon the Si content shown in Figure 9 cannot contribute to the sharp kink in the experimentally measured resistivity *vs.* Si content dependence. On the other hand, the derivative of the density of states at the Fermi level presented in Figure 10, demonstrates a maximum as a function of Si content, more pronounced under pressure as high as 16 GPa. This behavior correlates qualitatively with the maximum in the concentration dependence of the experimentally measured thermoelectric power [7]. However, fitting the calculated concentration dependence of $[\mathrm{d}N(E)/\mathrm{d}E]_{E=E_F}$ to experimental data one finds that the experimental maximum is much sharper and cannot be accounted for from the $[\mathrm{d}N(E)/\mathrm{d}E]_{E=E_F}$ dependence only. When calculating an additional contribution to the thermoelectric power coming from $[\partial\tau/\partial E]_{E=E_F}$ from equation (1), we find the quantitative agreement between theory and experiment

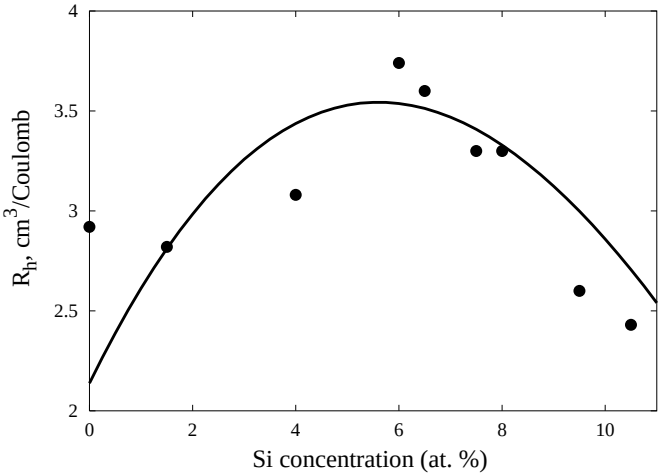

Fig. 13. Calculated Hall constant as a function of Si content: the circles are experimental data from reference [7], solid line is a fit.

as demonstrated in Figure 12. The quality of the fit is worse for Hall constant R (Fig. 13) since according to equation (3), R does not contain the relaxation time and is governed by the density of states and its derivative only. The poor quality of the fit for Hall constant may indicate that the theory of Hall effect in substitutional solid solutions should be revised.

6 Conclusions

Summarizing, we presented results of our theoretical calculations of the Fermi surfaces, the thermodynamic properties as well as the resistivity, the thermoelectric power and Hall constant of Al_xSi_{1-x} solid solutions. A first-principles study demonstrates how essential the effect of substitution of Al for Si is for the electronic properties of this material. In particular, two electronic topological transitions were predicted for the system upon applying pressure and upon alloying with Si. The other remarkable feature of the electronic structure is the nesting which becomes more pronounced upon Si doping. We studied the behavior of the alloy formation enthalpy, lattice parameter and bulk modulus and demonstrated the agreement between our calculated results and available experimental data. Further, we calculated the one-electron density of states and its energy derivative at the Fermi level and showed that changes in $N(E_F)$ and $[\mathrm{d}N(E)/\mathrm{d}E]_{E=E_F}$ cannot account for the peculiarities in transport properties. A consistent description of unusual transport properties in Al_xSi_{1-x} solid solutions is provided by the consideration of the anomalous electron relaxation time in the proximity of the ETT, while enhanced superconductivity is attributed to the flattening of the Fermi surface parts followed by nesting effects. In this respect it is worth to emphasize that though the enhancement of the electron-phonon interaction in the vicinity of the lattice instability

point could be the main factor responsible for the T_c increase, there is a solid ground to believe that anomalies in the transport properties of metastable $Al_{1-x}Si_x$ alloys are mainly due to the ETT, so the reasons for the two effects are different.

The authors acknowledge the support from The Royal Swedish Academy of Sciences (KVA), the Russian Foundation of Basic Research under grants # 99-02-16067 and 02-02-16006, and the Netherlands Organization for Scientific Research (NWO) under grant # 047-008-016.

References

1. V.F. Degtyareva, G.V. Chipenko, I.T. Belash, O.I. Barkalov, E.G. Ponyatovskii, Phys. Status Solidi A **89**, K127 (1985).
2. J. Chevrer, J.B. Suck, J.C. Lasjaunias, M. Perroux, Phys. Rev. B **49**, 961 (1994).
3. J. Chevrer, J.B. Suck, J.J. Capponi, M. Perroux, Phys. Rev. Lett. **61**, 554 (1988).
4. A. Caro, D.A. Prabold, O.F. Sankey, Phys. Rev. B **49**, 6647 (1994).
5. N.E. Sluchanko, V.V. Glushkov, S.V. Demishev, M.V. Kondrin, N.A. Samarin, V.V. Brazhkin, Y. Bruynseraede, V.V. Moshchalkov, Sov. Phys. Solid State **41**, 3 (1999).
6. N.E. Sluchanko, V.V. Glushkov, S.V. Demishev, N.A. Samarin, S.V. Savchenko, J. Singleton, W. Hayes, V.V. Brazhkin, A.A. Gippius, A.I. Shulgin, Phys. Rev. B **51**, 1112 (1995).
7. N.E. Sluchanko, V.V. Glushkov, S.V. Demishev, M.V. Kondrin, N.A. Samarin, V.V. Moshchalkov, V.V. Brazhkin, Sov. Phys. JETP **113**, 339 (1998).
8. N.E. Sluchanko, V.V. Glushkov, S.V. Demishev, M.V. Kondrin, N.A. Samarin, V.V. Brazhkin, Y. Bruynseraede, V.V. Moshchalkov, Sov. Phys. Solid State **41**, 1 (1999).
9. A.A. Gippius, N.E. Sluchanko, V.V. Glushkov, S.V. Demishev, M.V. Kondrin, A.A. Pronin, V.V. Brazhkin, Y. Bruynseraede, V.V. Moshchalkov, J. Phys. Cond. Matt. **12**, 1 (2000).
10. I.A. Abrikosov, B. Johansson, Phys. Rev. B **57**, 14164 (1998).
11. J.P. Perdew, K. Burke, M. Ernzerhof, Phys. Rev. Lett. **77**, 3865 (1996).
12. P.A. Korzhavyi, A.V. Ruban, I.A. Abrikosov, H.L. Skriver, Phys. Rev. B **51**, 5773 (1995).
13. V.L. Moruzzi, J.F. Janak, K. Schwarz, Phys. Rev. B **37**, 790 (1988).
14. N.V. Skorodumova, S.I. Simak, I.A. Abrikosov, B. Johansson, Y.Kh. Vekilov, Phys. Rev. B **57**, 14673 (1998).
15. W. Kohn, Phys. Rev. Lett. **2**, 393 (1959).
16. D.J. Scalapino, E. Loh, J.E. Hirsch, Phys. Rev. B **35**, 6694 (1987).
17. L.P. Gorkov, O.N. Dorokhov, J. Low Temp. Phys. **22**, 1 (1976).
18. A.A. Varlamov, V.S. Egorov, A.V. Pantsulaya, Adv. Phys. **38**, 469 (1989).
19. D. Ludecke, Z. Metallkde **77**, 278 (1986).
20. H. Olijnyk, S.K. Sikka, W.B. Holzapfel, Phys. Lett. A **103**, 137 (1984).
21. J.Z. Hu, L.D. Merkel, C.S. Menoni, I.L. Spain, Phys. Rev. B **34**, 4679 (1989).
22. V.F. Degtyareva, G.V. Chipenko, I.T. Belash, O.I. Barkalov, E.G. Ponyatovskii, Phys. Status Solidi A **89**, K127 (1985).
23. N.E. Sluchanko, V.V. Glushkov, S.V. Demishev, M.V. Kondrin, T.V. Ischenko, W. Gust, V.V. Brazhkin, B.B. Straunal, Y. Bruynseraede, V.V. Moshchalkov, Phys. Rev. B **61**, 6019 (2000).
24. A.M. James, M.P. Lord, in *Macmillan's Chemical and Physical Data* (Macmillan, London, UK, 1992).
25. Ya.M. Blanter, M.I. Kaganov, A.V. Pantsulaya, A.A. Varlamov, Phys. Rep. **245**, 159 (1994).
26. A.A. Abrikosov, *Fundamentals of the Metals Theory* (North Holland, Elsevier, 1988).
27. D.V. Livanov, Phys. Rev. B **60**, 13439 (1999).